

Floquet-Bloch waves and suppression of vibrations in multi-scale fluid-solid systems

Giorgio Carta*, Luca P. Argani, Alexander B. Movchan

Department of Mathematical Sciences, University of Liverpool, UK

Abstract

The paper presents a mathematical model for an industry inspired problem of vibration isolation applied to a cluster of elastic fluid-filled containers. We develop a systematic approach employing full fluid-solid interaction and Floquet-Bloch waves in periodic multi-scale systems. The analytical findings are accompanied by numerical simulations, including frequency response analyses and computations in the transient regime.

Keywords: vibration isolation; multi-scale resonators; fluid-solid interaction; sloshing waves; Floquet-Bloch waves; dispersion analysis.

1 Introduction

Mathematical modelling of linear waves in fluids is a classical subject, which has generated a lot of interest among applied mathematicians, physicists and engineers. In particular, the classical texts by Ursell (1958, 1994) and Kuznetsov et al. (2002) present an excellent theoretical framework of linear water waves in the context of partial differential equations. The dynamics of sloshing is well described in the text by Ibrahim (2005), which provides elegant estimates of eigenfrequencies of sloshing waves in solid containers.

*Corresponding author. Email addresses: giorgio_carta@unica.it; luca.argani@unitn.it; abm@liverpool.ac.uk

In many engineering systems the fluid interacts with a deformable or a moving solid, in which case the coupling between the fluid and the solid needs to be taken into account in the design process. Fluid-solid interaction problems concerning vibrations of slender structures induced by axial flow are discussed in the comprehensive treatise by Païdoussis (1998, 2004). Banerjee and Kundu (2007) used the Distributed Point Source Method to derive the ultrasonic field created by ultrasonic transducers in a solid plate immersed in a fluid, and compared the analytical results with the Lamb wave modes visualised experimentally with stroboscopic photoelasticity. Cho et al. (2015) investigated the frequency response of plate structures in contact with a fluid under an internal harmonic force. Liao and Ma (2016) calculated the resonant frequencies and the associated mode shapes of a rectangular plate lying at the bottom of a container filled with inviscid compressible fluid.

Another important application involving fluid-solid interaction concerns wave propagation in deformable pipes, such as gas risers and blood vessels. Fuller and Fahy (1982) determined the dispersion properties and the energy distribution of waves in fluid-filled cylindrical pipes, modelled as shells. Sorokin et al. (2004) investigated dispersion and power flow in a cylindrical shell with and without internal fluid loading. Mencik and Ichchou (2007) presented a finite element formulation to compute the dispersion curves and the forced response of a generic elastic waveguide containing an acoustic fluid.

If the fluid inside a solid has a free surface, sloshing waves are generated when the system is subjected to a dynamic excitation. The frequencies of sloshing waves can be calculated analytically if the solid container is assumed to be rigid (see Ibrahim (2005)). On the other hand, when the container is elastic, numerical or experimental investigations are usually conducted. Jiang et al. (2014) performed an experimental sweep test to determine the lower frequencies of sloshing waves in a tank with a prismatic base, considering both thick (rigid) and thin (elastic) walls, and they found that the resonant frequencies are very close to each other. Pal and Bhattacharyya (2010) proposed a meshless formulation based on the Petrov-Galerkin method to study non-linear sloshing waves in a prismatic container under harmonic base excitation, and they obtained a good agreement with the solutions given by Frandsen (2004) and Washizu et al. (1984). In engineering applications, the amplitudes of sloshing waves are usually attenuated by using baffles, as shown by Belakroum et al. (2010) and Wang et al. (2012).

The purpose of the present paper is to analyse Floquet-Bloch type waves in large systems of fluid-filled containers and to offer a design leading to



Figure 1: (a) Array of tanks in a petrochemical plant (image taken from www.joc.com, accessed on 19/01/2016); (b) cylindrical steel tanks, used to storage water, resting on a concrete foundation (image taken from www.alibaba.com, accessed on 19/01/2016).

suppression of undesirable vibrations. The main applications are in the protection of storage tanks in industrial facilities (see Fig. 1), subjected to dynamic excitations such as seismic waves, which can cause serious accidents and endanger human life (Krausmann et al. (2010)).

In order to mitigate the vibrations of fluid-filled containers, we propose to introduce a novel system of high-contrast multi-scale resonators, made of many concentrated masses linked by light beams (see Fig. 2). This system is designed to re-distribute vibrations within a fluid-solid system in a predefined finite frequency range. The high-contrast multi-scale resonators can be tuned to serve the required frequency interval by varying the masses or the connecting beams. The proposed design is different from the conventional Tuned Mass Dampers, which are effective only around the eigenfrequency of the damper. The possibility to reduce the vibrations in a finite frequency interval is crucial when the spectrum of the system depends on a random parameter, such as the level of fluid inside the container. We also point out that the masses of the resonators can be much smaller than the mass of the fluid-filled container.

We begin by illustrating the use of the multi-scale resonators in the reduction of the vibrations of a three-dimensional cylindrical fuel tank, used in a petrochemical plant. The fluid-solid system and the design of the resonators are described in Section 2. A significant dynamic effect of the resonators on the tank is shown in Fig. 5. We continue by taking a large cluster of connected fluid-filled elastic containers, subjected to externally

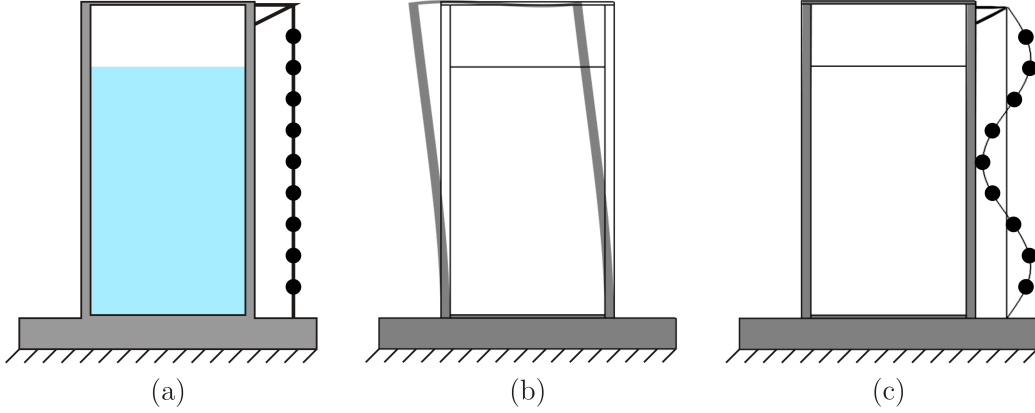


Figure 2: (a) Scheme of a chain of multi-scale resonators connected to a solid container filled with fluid; (b) first eigenmode of the fluid-filled container without the resonators; (c) eigenmode of the system with the resonators. It is apparent that the resonators are capable of diverting the vibrations away from the main structure. The simulations are carried out taking into account the full interaction between solid and fluid.

induced vibrations, as discussed in Section 3. A set of many containers is an interesting scenario, considering that in an industrial plant there are areas covered by many tanks connected to each other (see Fig. 1). In the periodic approximation for Floquet-Bloch waves describing lateral motion of the connected containers, we deduce a dispersion relation and construct dispersion diagrams, which clearly show existence of stop-bands as well as standing waves in this multi-scale structure, which incorporates fluid-solid interaction. As a part of the model, we present several approximations to estimate the resonant frequencies of the combined fluid-solid system. In Section 4 we discuss a simplified approach, whereby the fluid is modelled by masses connected to the elastic structure by springs. Eigenfrequency computations show that this approach provides an approximate estimate of the natural frequencies of the fluid-solid system. We conclude by presenting in Section 5 analytical results of sloshing waves in three-dimensional and two-dimensional containers. We also perform some numerical simulations to assess the effect of the multi-scale resonators on the sloshing waves in the fluid. Finally, in Section 6 we provide some concluding remarks.

2 Vibration isolation of cylindrical tanks filled with fluid

Tanks in an industrial plant, used to store flammable gases or liquids, are generally designed as steel cylinders with small thickness. If the plant is located in a region of high seismicity, the tanks need to resist strong earthquakes without serious damage.

In this Section, we study a typical slender cylindrical tank containing petrol (see Fig. 3a). The tank has radius $r = 4$ m, height $h_T = 14$ m and thickness $t_T = 0.006$ m. It is made of steel, having the following properties: Young's modulus $E_s = 190$ GPa, Poisson's ratio $\nu_s = 0.3$ and density $\rho_s = 7870$ kg m⁻³. At the top the tank is covered by a steel lid of thickness $t_L = 0.08$ m, pinned to the tank. The fluid, which is assumed to have a height $h_P = 12$ m in the computations, is characterised by a bulk modulus $K_f = 1.3$ GPa, a density $\rho_f = 750$ kg m⁻³ and a dynamic viscosity $\mu_f = 0.0006$ Pa s. Since K_f is very large and μ_f is very small, the fluid can be considered as incompressible and inviscid. The foundation, which is a square block of side $l_F = 12$ m and thickness $h_F = 1$ m, is made of concrete, having a Young's modulus $E_c = 30$ GPa, a Poisson's ratio $\nu_c = 0.2$ and a density $\rho_c = 2500$ kg m⁻³.

2.1 Governing equations of the fluid-solid system

For an incompressible fluid with uniform density ρ_f and dynamic viscosity μ_f , the continuity equation and the Navier-Stokes equations have the following expressions:

$$\nabla \cdot \mathbf{v}_f = 0, \quad (1a)$$

$$\frac{\partial \mathbf{v}_f}{\partial t} + (\mathbf{v}_f \cdot \nabla) \mathbf{v}_f + \frac{\nabla p}{\rho_f} - \frac{\mu_f}{\rho_f} \nabla^2 \mathbf{v}_f = -g \mathbf{k}, \quad (1b)$$

where \mathbf{v}_f is the velocity field in the fluid, p is the pressure, g is the acceleration of gravity and \mathbf{k} is the unit vector in the z direction. The equations of motion of the elastic tank and foundation are given by

$$\mu_s \nabla^2 \mathbf{u}_T + (\lambda_s + \mu_s) \nabla \nabla \cdot \mathbf{u}_T = \rho_s \frac{\partial^2 \mathbf{u}_T}{\partial t^2} \quad (\text{steel tank}), \quad (2a)$$

$$\mu_c \nabla^2 \mathbf{u}_F + (\lambda_c + \mu_c) \nabla \nabla \cdot \mathbf{u}_F = \rho_c \frac{\partial^2 \mathbf{u}_F}{\partial t^2} \quad (\text{concrete foundation}). \quad (2b)$$

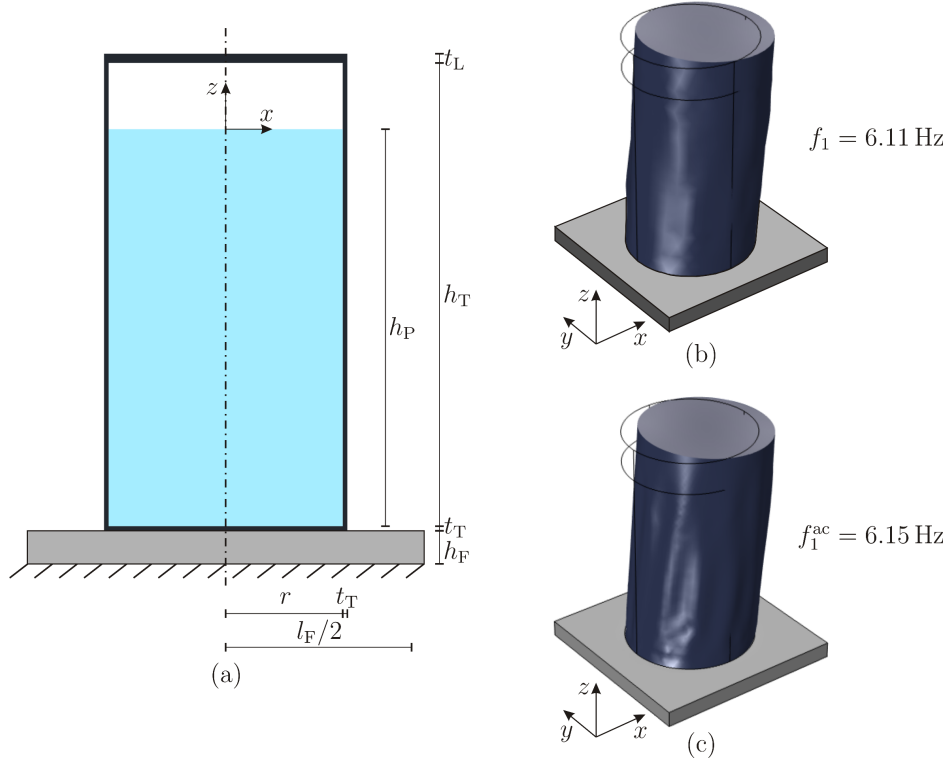


Figure 3: (a) Geometry of the three-dimensional cylindrical tank with fluid; first eigenmode and corresponding eigenfrequency of the fluid-filled tank obtained with the model based on the linearised Navier-Stokes equations (b) and with the acoustic approximation (c).

Here \mathbf{u}_T and \mathbf{u}_F denote the displacement vectors of the tank and the foundation, while $\mu_\alpha = E_\alpha / [2(1 + \nu_\alpha)]$ and $\lambda_\alpha = E_\alpha \nu_\alpha / [(1 + \nu_\alpha)(1 - 2\nu_\alpha)]$ (where $\alpha = c, s$) are the Lamé constants for the two materials.

The boundary conditions of the fluid-solid system are the following:

$$\mathbf{v}_f \cdot \mathbf{n} = \frac{\partial \mathbf{u}_T}{\partial t} \cdot \mathbf{n} \quad \text{at the interfaces fluid-solid,} \quad (3a)$$

$$\boldsymbol{\sigma}_T \mathbf{n} = -p \mathbf{n} \quad \text{at the interfaces fluid-solid,} \quad (3b)$$

$$p = p_0 \quad \text{on the fluid free surface,} \quad (3c)$$

$$\mathbf{u}_T = \mathbf{u}_F, \boldsymbol{\sigma}_T = \boldsymbol{\sigma}_F \quad \text{at the interfaces tank-foundation,} \quad (3d)$$

$$\mathbf{u}_F = \bar{\mathbf{u}} \quad \text{at the bottom of the foundation,} \quad (3e)$$

where $\boldsymbol{\sigma}_T$ and $\boldsymbol{\sigma}_F$ are the stress tensors in the tank and in the foundation, p_0 is the atmospheric pressure and \mathbf{n} is the normal unit vector. The displacement vector $\bar{\mathbf{u}}$ at the bottom of the foundation is assumed to be given. In the computations carried out in the transient regime, the system is assumed to be at rest at the initial time.

2.2 Frequency response of the cylindrical tank

We determine the eigenfrequencies and eigenmodes of the fluid-solid system by employing two approaches, based on different formulations of the fluid domain. In the first approach we simplify the governing equations of the system in the framework of the *linear water wave theory*, while in the second formulation we approximate the fluid as an acoustic medium. In Section 4 we will discuss an alternative method, in which the fluid is modelled by spring-mass oscillators, and we will show that this method, that is widely used in the literature, can lead to an imprecise evaluation of the eigenfrequencies of the fluid-solid system.

2.2.1 Simplified governing equations

In order to perform an eigenfrequency analysis, we need to remove the non-linear and viscous terms from the Navier-Stokes equations (1b). We consider small harmonic oscillations around the equilibrium configuration, such that $\mathbf{v}_f = \mathbf{V}_f + \tilde{\mathbf{v}}_f e^{i\omega t}$ and $p = P + \tilde{p} e^{i\omega t}$, where ω is the radian frequency. At equilibrium the fluid is quiescent ($\mathbf{V}_f = \mathbf{0}$) and P is the hydrostatic pressure

($P = \rho_f g |z|$). The amplitudes of the fluid variables are obtained from the following equations:

$$\nabla \cdot \tilde{\mathbf{v}}_f = 0, \quad (4a)$$

$$i\omega \tilde{\mathbf{v}}_f + \frac{\nabla \tilde{p}}{\rho_f} = \mathbf{0}. \quad (4b)$$

For conciseness, the time factor $e^{i\omega t}$ is suppressed throughout the paper. After imposing time-harmonic conditions, the equations of motion of the elastic solids (2) become

$$\mu_s \nabla^2 \tilde{\mathbf{u}}_T + (\lambda_s + \mu_s) \nabla \nabla \cdot \tilde{\mathbf{u}}_T + \rho_s \omega^2 \tilde{\mathbf{u}}_T = \mathbf{0} \quad (\text{steel tank}), \quad (5a)$$

$$\mu_c \nabla^2 \tilde{\mathbf{u}}_F + (\lambda_c + \mu_c) \nabla \nabla \cdot \tilde{\mathbf{u}}_F + \rho_c \omega^2 \tilde{\mathbf{u}}_F = \mathbf{0} \quad (\text{concrete foundation}). \quad (5b)$$

The boundary conditions (3) are changed into

$$\tilde{\mathbf{v}}_f \cdot \mathbf{n} = i\omega \tilde{\mathbf{u}}_T \cdot \mathbf{n} \quad \text{at the interfaces fluid-solid}, \quad (6a)$$

$$\tilde{\boldsymbol{\sigma}}_T \mathbf{n} = -\tilde{p} \mathbf{n} \quad \text{at the interfaces fluid-solid}, \quad (6b)$$

$$\tilde{p} = 0 \quad \text{on the fluid free surface}, \quad (6c)$$

$$\tilde{\mathbf{u}}_T = \tilde{\mathbf{u}}_F, \quad \tilde{\boldsymbol{\sigma}}_T = \tilde{\boldsymbol{\sigma}}_F \quad \text{at the interfaces tank-foundation}, \quad (6d)$$

$$\tilde{\mathbf{u}}_F = \bar{\mathbf{u}} \quad \text{at the bottom of the foundation}. \quad (6e)$$

The eigenfrequencies and eigenmodes of the fluid-solid system are computed by means of a finite element model developed in *Comsol Multiphysics*[®] (version 5.1), where the tank is modelled as a shell to simplify the computations. The bottom of the foundation is assumed to be fixed ($\bar{\mathbf{u}} = \mathbf{0}$ in Eq. (6e)). The first antisymmetric eigenmode is shown in Fig. 3b, and it corresponds to an eigenfrequency $f_1 = 6.11$ Hz. We focus the attention on the antisymmetric modes of the system, since they are the only modes excited by a horizontal acceleration of the ground (Graham and Rodriguez (1952)), as in the presence of an earthquake.

2.2.2 Acoustic approximation

The second approach that we follow consists in modelling the fluid as an acoustic medium, characterised by the following equation of motion in the transient regime:

$$K_f \nabla^2 p = \rho_f \frac{\partial^2 p}{\partial t^2}, \quad (7)$$

which under time-harmonic conditions takes the form:

$$K_f \nabla^2 \tilde{p} + \rho_f \omega^2 \tilde{p} = 0. \quad (8)$$

In this case, the boundary condition (3a) or (6a) needs to be removed from the formulation of the problem.

The present approach represents an approximation of the method described in Section 2.2.1, since the velocity is not a variable of the problem so that the fluid flow is neglected. Only pressure waves propagate in the fluid, as the latter is assumed to be inviscid.

The first eigenfrequency associated with an antisymmetric mode, shown in Fig. 3c, is found to be $f_1^{ac} = 6.15$ Hz, which is very close to the value determined with the linear water wave theory. The reason is that the frequencies of sloshing waves are considerably smaller than 6.15 Hz (see 5.1), therefore the contribution of the fluid velocity can be ignored. On the other hand, at low frequencies the model based on the linearised Navier-Stokes equations should be employed, since in this case the velocity of sloshing waves is significant.

2.3 Design of multi-scale resonators

In order to reduce the vibrations of the tank induced by earthquakes, we propose to insert a passive system of high-contrast multi-scale resonators. When the fluid-solid system is subjected to a dynamic base excitation characterised by a Fourier spectrum having a peak around a frequency close to one of the eigenfrequencies of the resonators, the latter start to vibrate, while the oscillations of the main structure are reduced. In this way, waves are diverted away from the tank, which undergoes smaller deformations and is subjected to lower stresses and displacements. We observe that the lower modes of the resonators are more efficient, as they require more energy to vibrate.

The system of resonators consists of four chains of masses m , two in the x direction and two in the y direction, linked by light flexural elements with uniform length d and flexural stiffness EJ (see Figs. 4a and 4b). The chains are pinned at the bottom to the concrete foundation and at the top to a truss made of bars with high rigidity, which is connected to the tank.

If the number of masses is large enough, each chain of resonators can be studied analytically as a periodic structure made of point masses connected by non-inertial beams. This periodic structure is characterised by a single

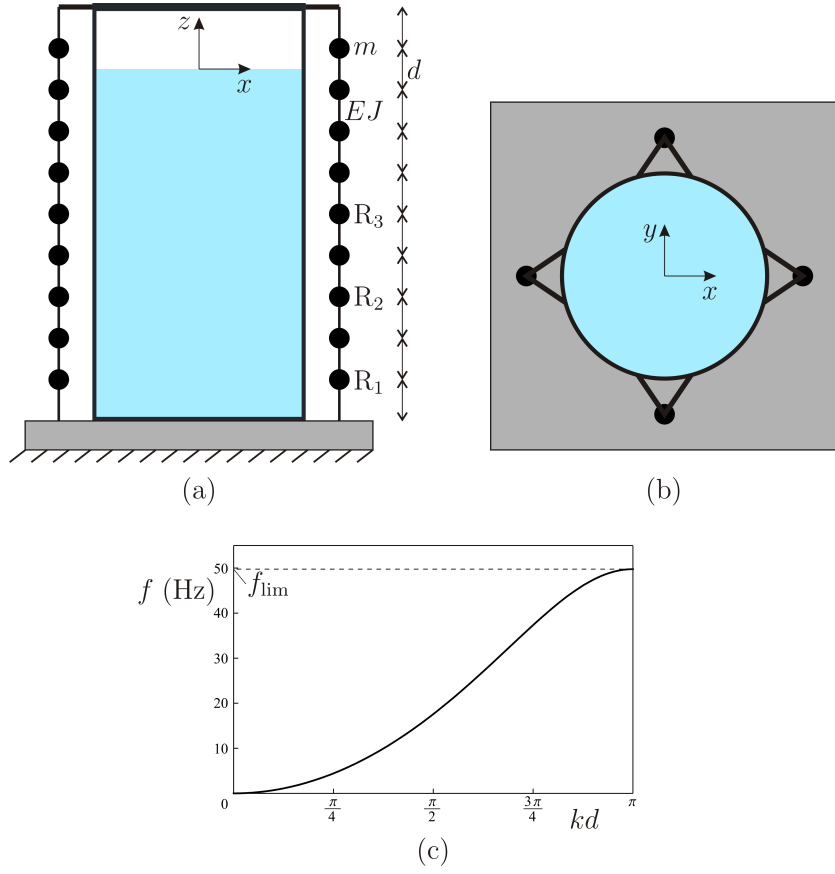


Figure 4: Proposed system of multi-scale resonators: front section (a) and top view (b); dispersion curve of the system of resonators analysed as a periodic structure (c).

dispersion curve, which has the following expression (Carta et al. (2016)):

$$\omega = \sqrt{\frac{6EJ[3 + \cos(2kd) - 4\cos(kd)]}{md^3[2 + \cos(kd)]}}, \quad (9)$$

where k is the wavenumber. The upper limit of this dispersion curve is $\omega_{\text{lim}} = 4\sqrt{3EJ/(md^3)}$. If the system of resonators is made of a finite number of masses, as in reality, its eigenfrequencies lie inside the pass-band of the periodic structure, for any boundary conditions imposed at the ends (see also Mead (1996) and Carta et al. (2014a)).

Eq. (9) allows to determine precisely the frequency interval where the resonators are effective. The upper limit ω_{lim} of this frequency interval can be easily modified by changing the masses or the properties of the beams. The capability of the resonators to work in a large frequency range is very important when the natural frequencies of the system can vary during its service life, as in the present case due to the variation of the fluid level inside the tank: this is the main advantage of the proposed design. We also point out that the number of the eigenfrequencies of the resonators, around which the resonators are more efficient, can be increased by adding more masses.

For the tank examined in this Section, we design each chain of resonators as made of nine steel spheres of radius 0.26 m. The masses are connected to each other by steel beams of length 1.4 m and hollow circular cross-section of outer radius equal to 0.085 m and inner radius equal to 0.075 m. The elastic modulus, Poisson's ratio and density of steel used for the resonators are equal to 200 GPa, 0.3 and 7850 kg m^{-3} , respectively. We note that the mass of each beam is much smaller than the mass of each sphere. Moreover, the total mass of the four chains of resonators is less than 4% of the total mass of the tank completely filled with petrol. The dispersion curve obtained from Eq. (9) is shown in terms of the frequency f and the normalised wavenumber kd in Fig. 4c, where the upper limit is $f_{\text{lim}} = \omega_{\text{lim}}/(2\pi)$.

2.3.1 Effect of multi-scale resonators on the transient response of the tank

In order to assess the efficiency of the proposed system of resonators, we carry out numerical simulations in the transient regime. We model the fluid as an acoustic medium using Eq. (7), because at high frequencies the velocity of sloshing waves is negligible, as demonstrated in Section 2.2.2. This

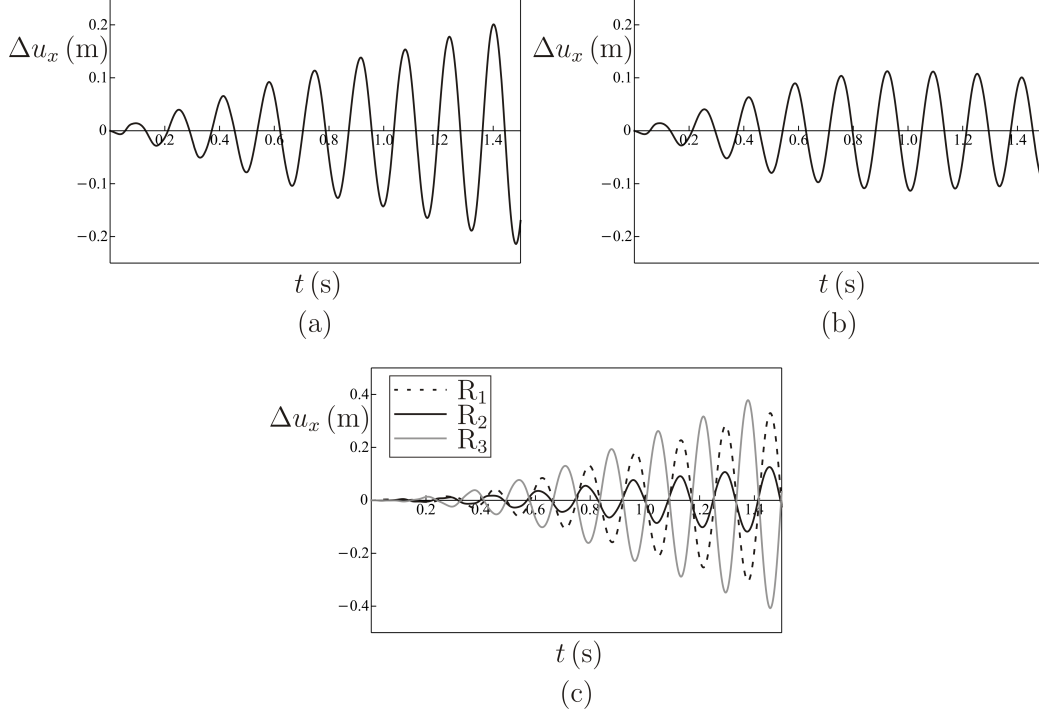


Figure 5: Time-histories of the relative displacement along the x direction between the top and the bottom of the tank at $f = 6.1$ Hz, in absence of resonators (a) and when the resonators are attached to the tank (b); time-histories of the displacements of resonators R_1 , R_2 and R_3 (c), indicated in Fig. 4a.

simplification allows to perform the simulations at an affordable computational cost.

We impose a sinusoidal displacement in the x direction at the bottom of the foundation, given by $u_x^B = d_0 \sin(2\pi ft)$, where $d_0 = 0.005$ m is the amplitude, $f = 6.1$ Hz is the frequency and t is time. By using a finite element model built in *Comsol Multiphysics*[®], we compute the time-history of the relative displacement in the x direction between the top and the bottom of the tank, namely $\Delta u_x = u_x^T - u_x^B$, both when the resonators are absent and when they are installed.

The relative displacement Δu_x in the system without resonators is plotted in Fig. 5a. From this diagram it is apparent that Δu_x increases unbounded with time, because the forcing frequency is close to the natural frequency of the tank and damping has not been included in the computations.

Fig. 5b shows the time-history of the relative displacement Δu_x after

the resonators have been introduced. The displacements of three resonators, labelled as R_1 , R_2 and R_3 in Fig. 4a, are plotted in Fig. 5c. They increase unlimited in time because the chosen value of the imposed frequency is close to the one of the eigenfrequencies of the system of resonators, more specifically the third one. Figs. 5a-5c show that the resonators redistribute the vibrational energy produced by the external source, so that in the main structure the vibration amplitudes are decreased and resonant effects disappear. The resonators work well also if the frequency is close to – but not coincident with – one of their natural frequencies.

3 Waves in periodic systems of fluid-filled containers

In an industrial facility some areas are usually covered by sets of fuel storage tanks, connected to each other by the piping system or through the soil. In regions of high seismicity, it is essential to study how these sets of tanks behave when they are subjected to an earthquake and how their vibrations can be reduced in order to avoid serious accidents due to structural failure.

For simplicity we look at two-dimensional systems, because numerical simulations with several three-dimensional cylindrical tanks would require industrial scale computations. Nonetheless, the ideas and the procedures presented in this Section can be easily extended to three-dimensional geometries.

3.1 Two-dimensional models for fluid-solid interaction in the frequency domain

In order to determine the eigenfrequencies and eigenmodes of the two-dimensional system of containers, we employ the same approaches used in Section 2.2 for the three-dimensional cylindrical tank.

We assume that each container of the system has a rectangular section (see Fig. 6a) and unit thickness in the z direction, orthogonal to the xy plane. It is made of concrete, having Young's modulus $E_c = 30$ GPa, Poisson's ratio $\nu_c = 0.2$ and density $\rho_c = 2500$ kg m⁻³. The height and the half-width of the container are given by $h_T = 10$ m and $l_T = 2.5$ m, respectively, while the thickness of the walls is $t_T = 0.3$ m. The container is rigidly connected to a lid of thickness $t_L = 0.1$ m, which is also the thickness of the bottom.

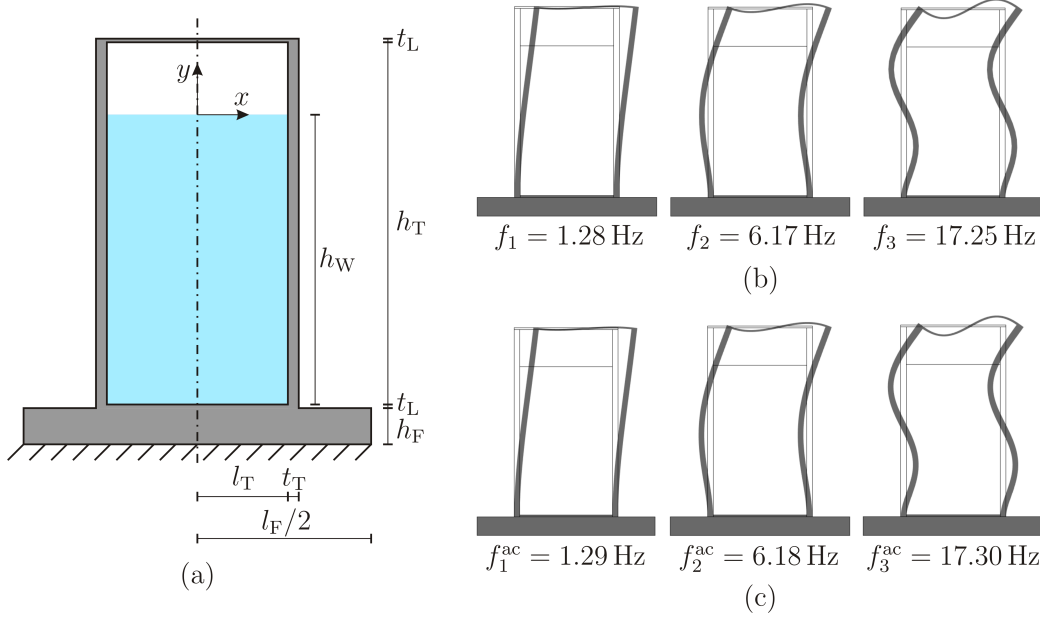


Figure 6: (a) Geometrical details of each fluid-filled container; first three antisymmetric eigenmodes and corresponding eigenfrequencies of a single container, obtained with the linear water wave theory (b) and with the acoustic approximation (c).

The container stands on a concrete foundation, having for simplicity the same constitutive properties as the container, with height $h_F = 1.0$ m and width $l_F = 9.6$ m. The fluid is assumed to have the properties of water, with density $\rho_f = 1000 \text{ kg m}^{-3}$, bulk modulus $K_f = 2.2 \text{ GPa}$ and dynamic viscosity $\mu_f = 0.001 \text{ Pa s}$, hence it can be studied as incompressible and inviscid. In the computations, the height of the fluid is taken as $h_W = 8$ m.

3.1.1 Simplified governing equations in the two-dimensional formulation

In the frequency domain, we neglect the contributions of the non-linear and viscous terms in the Navier-Stokes equations and we consider small harmonic oscillations around the equilibrium configuration, where the amplitudes of velocity and pressure are $\tilde{\mathbf{v}}_f$ and \tilde{p} respectively. The latter are described by

$$\nabla \cdot \tilde{\mathbf{v}}_f = 0, \quad (10a)$$

$$i\omega \tilde{\mathbf{v}}_f + \frac{\nabla \tilde{p}}{\rho_f} = \mathbf{0}. \quad (10b)$$

The container and the foundation are modelled as elastic solids, governed by the following equations in the time-harmonic regime:

$$\mu_c \nabla^2 \tilde{\mathbf{u}}_S + (\lambda_c + \mu_c) \nabla \nabla \cdot \tilde{\mathbf{u}}_S + \rho_c \omega^2 \tilde{\mathbf{u}}_S = \mathbf{0}, \quad (11)$$

where $\tilde{\mathbf{u}}_S$ is the displacement field in the solid, while $\mu_c = E_c / [2(1 + \nu_c)]$ and $\lambda_c = E_c \nu_c / [(1 + \nu_c)(1 - 2\nu_c)]$ are the Lamé constants. The boundary conditions are summarised below:

$$\tilde{\mathbf{v}}_f \cdot \mathbf{n} = i\omega \tilde{\mathbf{u}}_S \cdot \mathbf{n}, \quad \tilde{\boldsymbol{\sigma}}_S \mathbf{n} = -\tilde{p} \mathbf{n} \quad \text{at the interfaces fluid-solid,} \quad (12a)$$

$$\tilde{p} = 0 \quad \text{on the fluid free surface,} \quad (12b)$$

$$\tilde{\mathbf{u}}_S = \bar{\mathbf{u}} \quad \text{at the bottom of the foundation,} \quad (12c)$$

where $\tilde{\boldsymbol{\sigma}}_S$ is the stress tensor in the solid and $\bar{\mathbf{u}}$ is a prescribed displacement vector.

The equations above are implemented in a finite element model developed in *Comsol Multiphysics*[®], in which the analysis is performed under plane strain conditions. The bottom of the foundation is assumed to be fixed, i.e. $\bar{\mathbf{u}} = \mathbf{0}$ in Eq. (12c). The first three antisymmetric eigenmodes and their associated eigenfrequencies for a single container are shown in Fig. 6b.

3.1.2 Acoustic approximation

In this approximate method the velocity of the fluid is neglected, implying that the fluid flow is not taken into account. The only variable defined in the fluid domain is the pressure, which is governed by Eq. (8) in the time-harmonic regime.

The first three eigenfrequencies related to antisymmetric eigenmodes of a single container are reported in Fig. 6c. By comparing Figs. 6b and 6c, we can notice that also in the two-dimensional case the acoustic approximation provides a good estimate of the natural frequencies of the fluid-solid system. This is due to the fact that the first resonant modes of sloshing waves are found at much lower values of the frequency (refer to 5.1 for details), consequently the contribution of fluid flow at higher frequencies is negligible.

3.2 Floquet-Bloch waves in a periodic system of containers

A set of many tanks can be studied as a periodic system, consisting of an infinite array of repetitive cells. The analysis of this system can be simplified

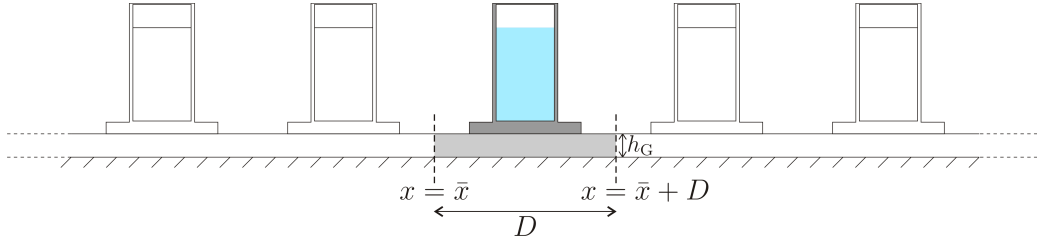


Figure 7: Identification of the repetitive cell in the periodic system of containers.

by studying a single cell with Floquet-Bloch boundary conditions. In this way, we can determine the dispersive properties of the system, in particular the frequency ranges where waves propagate without attenuation (*pass-bands*) and where they decay exponentially in space (*stop-bands*).

The interaction between the fluid and the solid is modelled by using the equations derived from the linear water wave theory (see Section 3.1.1), which gives the most accurate results and which can be handled numerically in the two-dimensional setting.

3.2.1 Periodic cell and quasi-periodicity conditions

We assume that the containers lie on a medium-dense sand soil, that is characterised by a Young's modulus $E_g = 70$ MPa, a Poisson's ratio $\nu_g = 0.25$ and a density $\rho_g = 2100$ kg m⁻³. The soil stands over a rigid layer of rock, hence we impose zero vertical displacements at the bottom of the sand layer. The repetitive cell of the system is indicated in Fig. 7, where $D = 15.6$ m is the distance between two adjacent cells and $h_G = 2$ m is the thickness of the sand layer.

At the ends of the periodic cell we apply Floquet-Bloch conditions:

$$\tilde{\mathbf{u}}(\bar{x} + D, y) = \tilde{\mathbf{u}}(\bar{x}, y) e^{ikD}, \quad (13)$$

where $\tilde{\mathbf{u}}$ is the displacement field and k is the wavenumber.

3.2.2 Dispersion curves

The dispersion curves of the periodic system in Fig. 7 are determined numerically by means of a finite element analysis. In particular, they are obtained by computing the eigenfrequencies of the periodic cell for several values of the

wavenumber, ranging within the first Brillouin zone. The dispersion curves show how the frequency f depends on the wavenumber k .

We consider three different levels of fluid, i.e. $h_W = h_T$, $h_W = h_T/2$ and $h_W = h_T/4$, where h_W and h_T denote the heights of the fluid and of the container respectively. The dispersion curves corresponding to these three cases are plotted in Fig. 8, where the solid lines represent the antisymmetric modes, the dashed lines the symmetric modes and the dotted lines the mixed modes. For each case, the dispersion curves associated with symmetric modes are almost flat, while those associated with mixed modes appear at higher frequencies.

The results in Fig. 8 show that, as the height of fluid is decreased, the dispersion curves move up towards higher frequencies. This result can be explained from a physical point of view considering that the eigenfrequencies of a system generally become larger if its mass is diminished. At the boundaries of the first Brillouin zone standing waves are observed, where the group velocity is zero. We also note that, for each case examined, there are large finite frequency intervals between the dispersion curves, which represent the stop-bands of the system, where waves cannot propagate.

3.3 Multi-scale resonators for the periodic system of containers

As shown in Fig. 8, the dispersion curves of the periodic system of containers can vary significantly with the level of fluid inside the containers. Therefore, in order to suppress or reduce the structural vibrations, we would need an isolation device that is effective in a large frequency interval. This purpose cannot be achieved with conventional Tuned Mass Dampers, which work well only in a narrow frequency range around the natural frequency of the damper. On the other hand, the system of resonators described in Section 2 is capable of mitigating the vibrations of the containers for many frequencies within a large interval, defined by the dispersion relation (9). The number of frequencies around which the resonators are efficient can be increased by adding more masses to the system.

We design the resonators in order to cover the interval $(0, 10)\text{Hz}$, where the dispersion curves related to the antisymmetric modes of the system of containers are found for very different values of fluid heights (see Fig. 8). The resonators, sketched in Fig. 9d for one container, are nine steel spheres

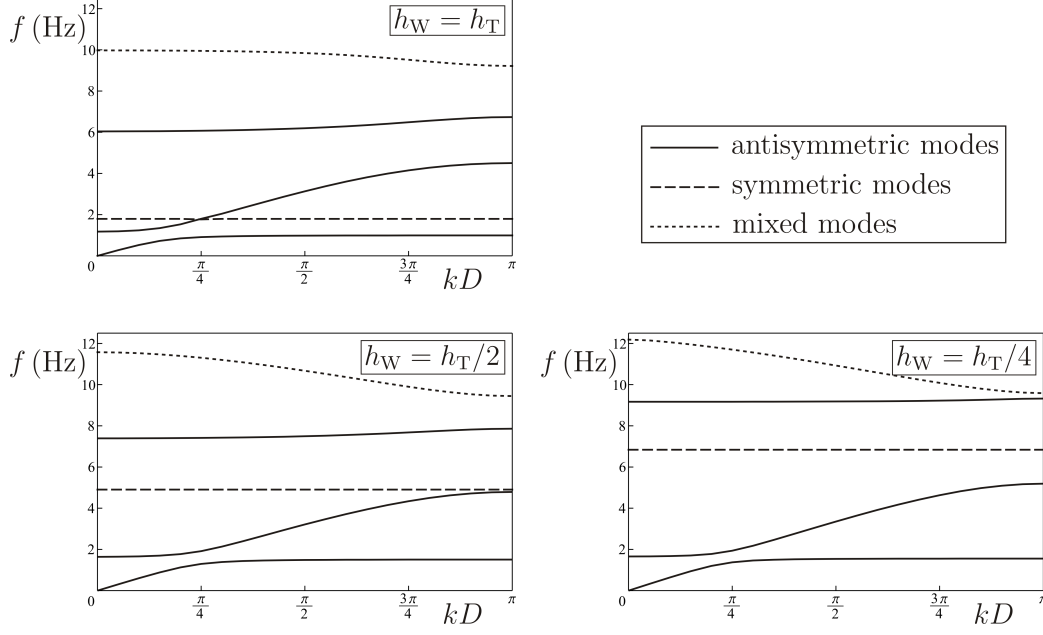


Figure 8: Dispersion curves for the periodic system of containers depicted in Fig. 7 without resonators, computed for three different levels of fluid.

of diameter 0.35 m, connected by steel beams of length 1 m and circular cross-section of diameter 0.035 m. The Young's modulus, Poisson's ratio and density of steel are $E_s = 200$ GPa, $\nu_s = 0.3$ and $\rho_s = 7850$ kg m⁻³, respectively. The system of resonators is linked to the top of the container by a rigid truss and tied to the foundation by a hinge. We point out that the mass of each beam is much smaller than the mass of each resonator, which justifies the approximation, used in the derivation of Eq. (9), that the beams can be analysed as non-inertial flexural elements. Furthermore, we note that the total mass of the system of resonators is less than 3% of the total mass of the fluid-filled container.

3.3.1 Application to a single container

We assess the performance of the resonators by carrying out some numerical simulations in the transient regime. In this case the motion of the fluid is governed by the complete Navier-Stokes equations (1b), which include both the convective and viscous terms. We consider first a single container and we assume that the solid and the fluid are at rest at $t = 0$. We apply a

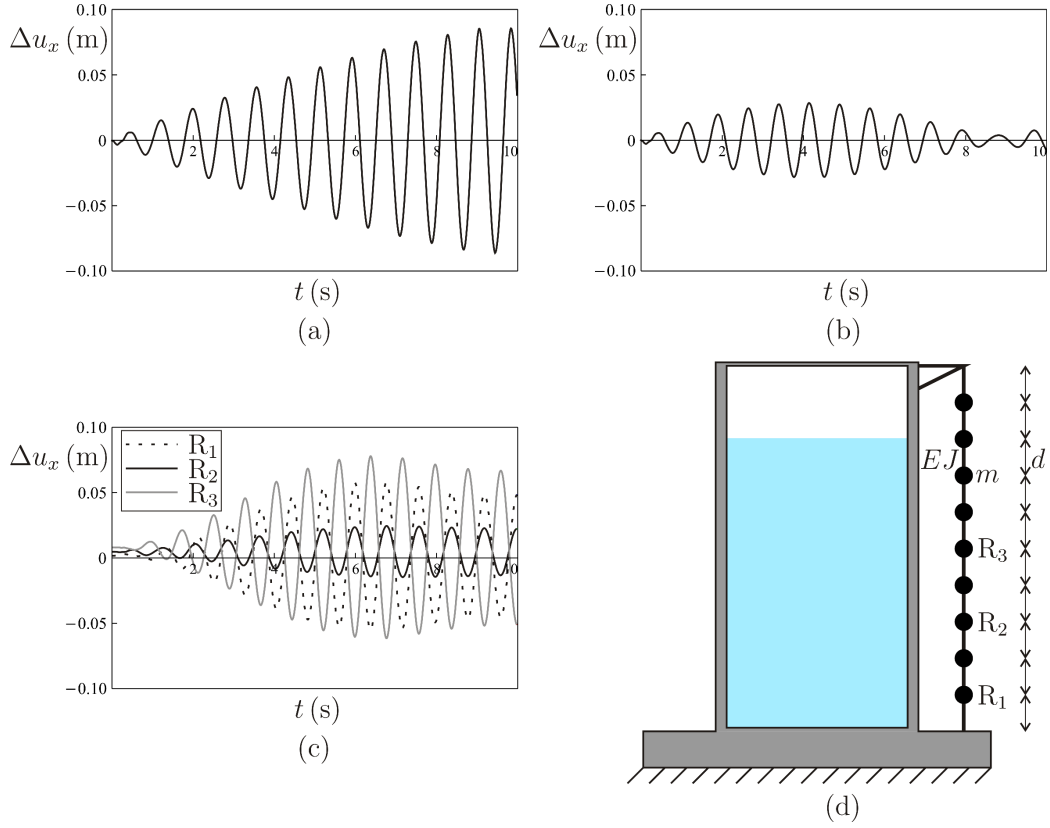


Figure 9: Time-histories of the relative horizontal displacement between the top and the bottom of a single container at $f = 1.28$ Hz in the case without resonators (a) and when resonators are introduced (b); (c) displacements versus time of resonators R_1 , R_2 and R_3 ; (d) schematic representation of the proposed system of resonators for a single container.

horizontal harmonic displacement at the bottom of the foundation, expressed by $u_x^B = d_0 \sin(2\pi ft)$, with $d_0 = 0.002$ m and $f = 1.28$ Hz, the latter being the first eigenfrequency of the fluid-solid system (see Fig. 6b). Then, we compute the horizontal displacement at the top of the container, indicated as u_x^T , and we calculate the relative displacement $\Delta u_x = u_x^T - u_x^B$.

If the resonators are absent, we obtain the diagram in Fig. 9a, which shows that the relative displacement between the top and the bottom of the container increases unbounded with time, since the frequency of the external excitation is close to the first eigenfrequency of the fluid-filled container. Resonance is detected also in correspondence of the second and third eigenfrequencies of the fluid-solid system, namely $f = 6.17$ Hz and $f = 17.25$ Hz (see Fig. 6b), which confirms the accuracy of the eigenfrequency analysis.

When the resonators are installed, the vibrations in the container decrease considerably and resonant effects disappear, as can be seen from the time-history of Δu_x in Fig. 9b. The reason is that most of the energy is absorbed by the resonators, which undergo large oscillations as shown in Fig. 9c. Indeed, the system of resonators has the following nine natural frequencies: 0.14 Hz, 0.56 Hz, 1.25 Hz, 2.25 Hz, 3.50 Hz, 4.98 Hz, 6.62 Hz, 8.24 Hz and 9.50 Hz, hence the resonant behaviour of the resonators is due to the fact that the applied frequency is close to their third eigenfrequency. The eigenmode corresponding to 1.25 Hz is shown in Fig. 2c.

3.3.2 Effect of the resonators on the dispersion properties of the periodic system of containers

If we connect the system of resonators to the container and we perform the dispersion analysis by imposing the quasi-periodicity conditions at the boundaries of the periodic cell, as described in Section 3.2.2, we find that new dispersion curves appear in correspondence of the modes of the resonators. These dispersion curves lie within the frequency interval (0, 10)Hz, in agreement with the design target. In Fig. 10 we present the results for the case $h_W = h_T/2$, namely when the containers are half-filled with fluid. Narrow stop-bands open up in proximity of the new dispersion curves, where waves decay exponentially; furthermore, standing waves are detected at the limits of the pass-bands.

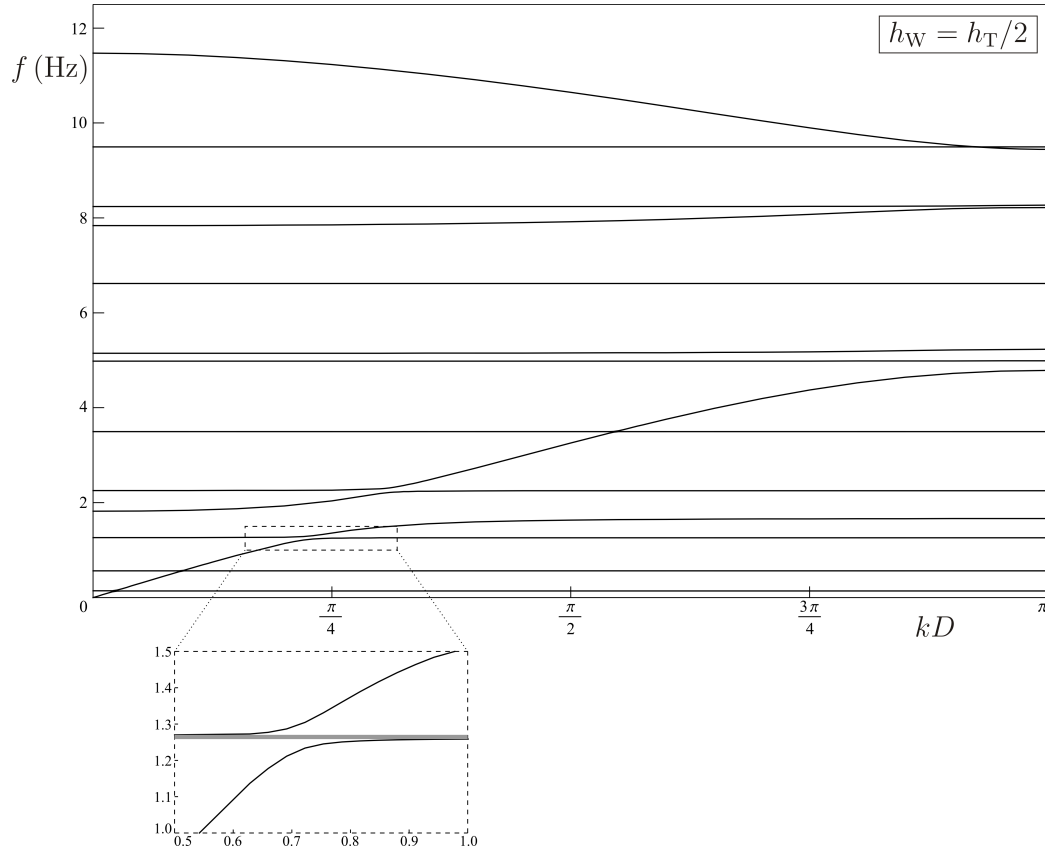


Figure 10: Dispersion curves for the periodic system of containers when the resonators are installed in the system, for the case $h_W = h_T/2$. The inset shows more clearly a stop-band created by the resonators, highlighted in grey.

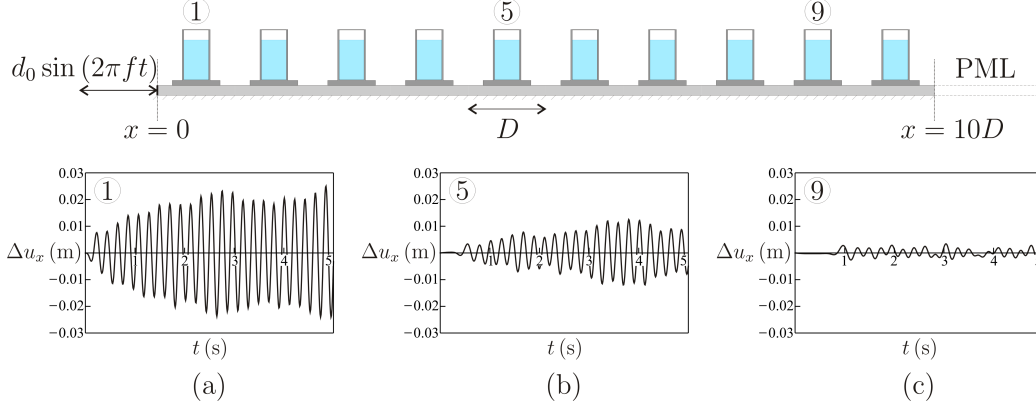


Figure 11: Time-histories of the relative displacements between the top and the bottom of the first, fifth and ninth containers of a semi-infinite set of containers, shown on top, evaluated near the limit of a stop-band ($f = 4.79$ Hz).

3.3.3 Effect of the resonators on the transient response of a system of containers

We analyse the transient response of a semi-infinite system of identical containers by referring to the dispersion properties of the corresponding periodic system, illustrated in Fig. 10. In the numerical computations we consider a set of ten containers connected by the soil layer, sketched at the top of Fig. 11. At the left boundary of the system ($x = 0$) we impose a harmonic horizontal displacement, given by $d_0 \sin(2\pi ft)$, with $d_0 = 0.002$ m and for different values of the frequency f . At the right boundary of the system ($x = 10D$) we attach a soil layer with viscous damping, which absorbs waves. In this way, reflections of waves at the right boundary of the system are avoided and the system behaves as semi-infinite. The layer with damping plays the role of a *Perfectly Matched Layer* (PML), in which the damping coefficient has been tuned in order to minimise reflections, as discussed in Carta et al. (2014b).

First, we consider an applied frequency equal to $f = 4.79$ Hz, which lies at the beginning of a stop-band (see Fig. 10). We determine the relative displacements Δu_x between the top and the bottom of the first, fifth and ninth containers, which are reported at the bottom of Fig. 11. It is apparent that the amplitude of Δu_x decreases considerably moving from the first to the ninth container, as expected since waves decay exponentially in space when the frequency is inside a stop-band.

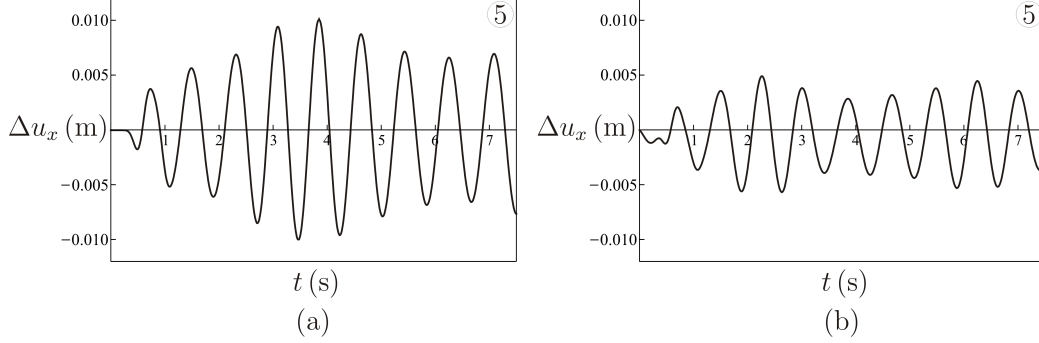


Figure 12: Time-histories of the relative displacements between the top and the bottom of the fifth container in a semi-infinite system without resonators (a) and with resonators (b), calculated at $f = 1.25$ Hz.

Next, we impose a harmonic horizontal displacement at $x = 0$ with a frequency $f = 1.25$ Hz, falling within a pass-band of the system (see Fig. 10). In Fig. 12a we plot the time-history of the relative displacement between the top and the bottom of the fifth container when the resonators are absent, while in Fig. 12b we illustrate the response of the fifth container after the resonators have been installed in the system. The comparison between the two cases shows that the resonators can reduce the structural vibrations of around 50%. The chosen value of the frequency is close to one of the flat dispersion curves produced by the resonators. Nonetheless, attenuation of waves has been observed also for other frequencies close to $f = 1.25$ Hz, namely at $f = 1.35$ Hz (refer to Fig. 17) and $f = 1.15$ Hz.

4 Discussion on the approximate spring-mass model for containers with sloshing waves

Approximate formulations have been proposed in the literature, whereby the fluid is modelled as a system of masses connected to the main structure by springs. This method, which is referred to as *spring-mass approximation*, is commonly used in practical applications, because it is simple and requires a lower computational cost. In this Section, we determine the eigenfrequencies of both the three-dimensional and two-dimensional fluid-filled containers by using the approximate spring-mass model, and we compare the results with the natural frequencies of the fluid-solid system derived from the approach based

on the linearised Navier-Stokes equations and from the acoustic approximation, discussed in the previous Sections.

4.1 Three-dimensional tank

For the three-dimensional tank studied in Section 2, we refer to the papers by Housner (1957, 1963) and Veletsos (1984). The fluid is represented by a mass M_0 , rigidly connected to the container, and by a mass M_1 , linked to the walls by an elastic spring of equivalent stiffness k_1 (see Fig. 13a). The positions of the masses with respect to the bottom of the tank are indicated by h_0 and h_1 , respectively. The expressions of these quantities are reported below:

$$M_0 = \frac{\tanh\left(\sqrt{3}\frac{r}{h_P}\right)}{\sqrt{3}\frac{r}{h_P}} M, \quad (14a)$$

$$h_0 = \frac{9}{20} h_P \quad \text{for } \frac{h_P}{r} > \frac{8}{3}, \quad (14b)$$

$$M_1 = \left(\frac{11}{24}\right)^2 \sqrt{\frac{27}{8}} \frac{r}{h_P} \tanh\left(\sqrt{\frac{27}{8}} \frac{h_P}{r}\right) M, \quad (14c)$$

$$k_1 = \frac{g}{r} \sqrt{\frac{27}{8}} \tanh\left(\sqrt{\frac{27}{8}} \frac{h_P}{r}\right) M_1, \quad (14d)$$

$$h_1 = \left[1 - \frac{\cosh\left(\sqrt{\frac{27}{8}} \frac{h_P}{r}\right) - \frac{135}{88}}{\sqrt{\frac{27}{8}} \frac{h_P}{r} \sinh\left(\sqrt{\frac{27}{8}} \frac{h_P}{r}\right)} \right] h_P, \quad (14e)$$

where $M = \pi r^2 h_P \rho_f$ is the total mass of the fluid.

The first antisymmetric mode, illustrated in Fig. 13b, is found at $f_1^{\text{sm}} = 6.44$ Hz. This value of the eigenfrequency is larger than the values determined with the more accurate methods based on the linearised Navier-Stokes equations and the acoustic approximation, presented in Sections 2.2.1 and 2.2.2 respectively (see Figs. 3b and 3c). Therefore, the spring-mass approximation should be employed only to have a rough estimate of the first eigenfrequency of the three-dimensional fluid-filled tank.

4.2 Two-dimensional container

The spring-mass approximation has been applied to two-dimensional containers in the works by Graham and Rodriguez (1952), Housner (1957), Li et

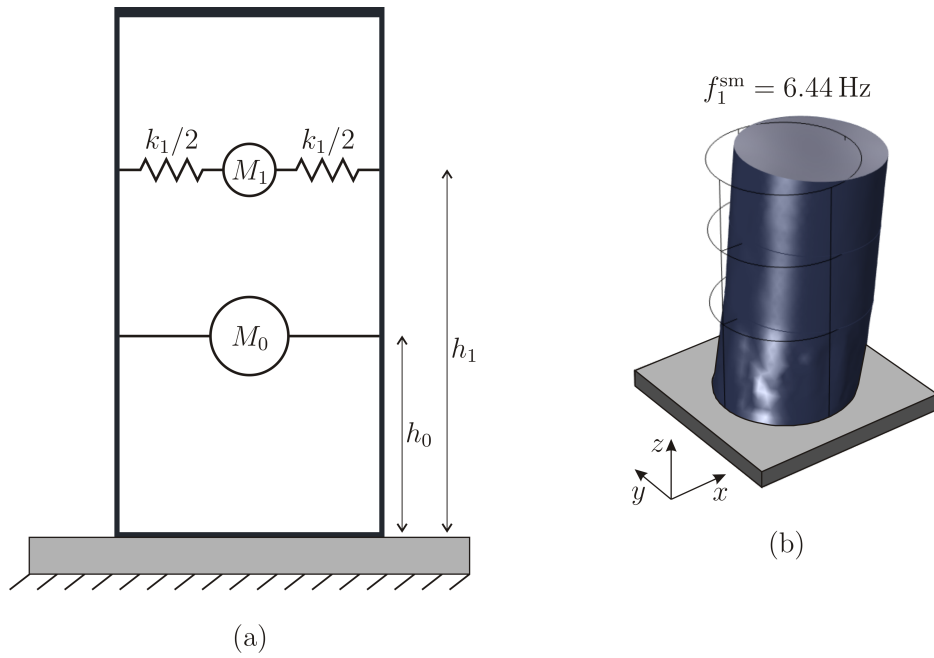


Figure 13: (a) Spring-mass approximation of the three-dimensional fluid-filled tank; (b) first eigenmode and eigenfrequency obtained with the spring-mass approximation.

al. (2012) and Bursi et al. (2015). For the rectangular container examined in Section 3 we consider the model by Li and Wang (2012), which is an improvement of the formulation provided by Graham and Rodriguez (1952). The fluid is represented by a mass M_0 , rigidly connected to the container, and by a set of spring-mass oscillators (M_n, k_n) ($n = 1, 2, \dots$) that simulate the sloshing modes of the fluid. We consider the case of two spring-mass oscillators, sketched in Fig. 14a. The positions of the masses M_0 , M_1 and M_2 with respect to the bottom of the tank are indicated by h_0 , h_1 and h_2 , respectively. The formulae for all the quantities indicated in Fig. 14a are reported below:

$$M_n = \frac{2(h_W/l_T)^2 \tanh(\beta_n h_W)}{(\beta_n h_W)^3} M \quad (n = 1, 2) , \quad (15a)$$

$$h_n = \left[1 + \frac{2 - \cosh(\beta_n h_W)}{\beta_n h_W \sinh(\beta_n h_W)} \right] h_W \quad (n = 1, 2) , \quad (15b)$$

$$M_0 = \left[1 - \sum_{n=1}^2 \frac{2(h_W/l_T)^2 \tanh(\beta_n h_W)}{(\beta_n h_W)^3} \right] M , \quad (15c)$$

$$h_0 = \frac{\frac{1}{2} + \frac{1}{3} \left(\frac{l_T}{h_W} \right)^2 - 2 \left(\frac{h_W}{l_T} \right)^2 \sum_{n=1}^2 \frac{2 + \beta_n h_W \sinh(\beta_n h_W) - \cosh(\beta_n h_W)}{(\beta_n h_W)^4 \cosh(\beta_n h_W)}}{1 - \sum_{n=1}^2 \frac{2(h_W/l_T)^2 \tanh(\beta_n h_W)}{(\beta_n h_W)^3}} h_W , \quad (15d)$$

$$k_n = M_n \omega_{(n)}^2 = \frac{2Mg}{h_W} \left(\frac{h_W}{l_T} \right)^2 \left[\frac{\tanh(\beta_n h_W)}{\beta_n h_W} \right]^2 \quad (n = 1, 2) . \quad (15e)$$

Here $\beta_n = (2n - 1)\pi/(2l_T)$, $\omega_{(n)}$ is the n -th frequency of the sloshing waves (given also by Eq. (19) in 5.1), and $M = 2l_T h_W \rho_f$ is the total mass per unit thickness of the fluid.

The first three antisymmetric eigenmodes and their corresponding eigenfrequencies obtained with the approximate spring-mass model are plotted in Fig. 14b. Comparing the results illustrated in Figs. 6b and 14b, we note that the spring-mass model does not provide a good estimate of the natural frequencies of the fluid-solid system, in particular for the second and third modes. We have checked that the accuracy of this approximation does not improve significantly by increasing the number of spring-mass oscillators.

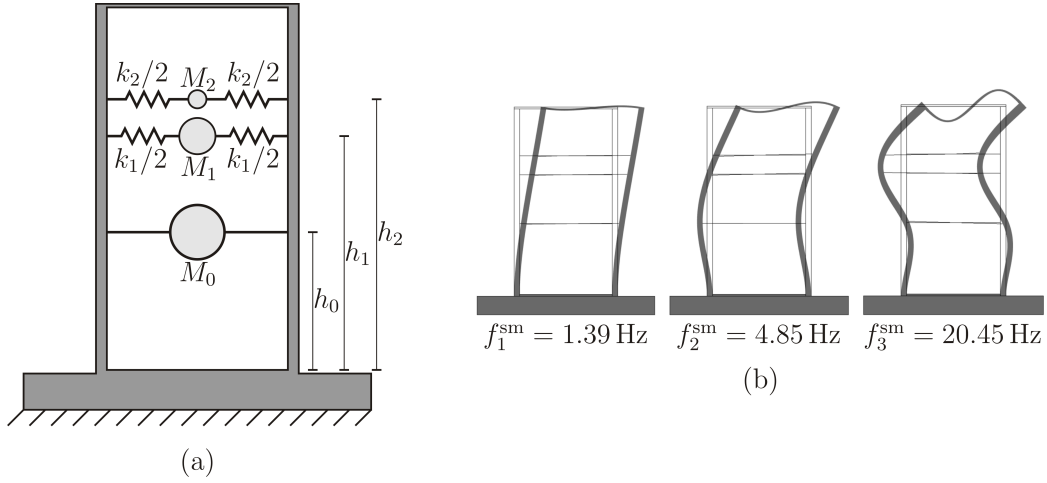


Figure 14: (a) Approximate spring-mass model for the two-dimensional fluid-filled container; (b) first three antisymmetric eigenmodes and relative eigenfrequencies derived from the approximate spring-mass model.

5 Analytical and numerical study of sloshing waves

The sloshing of the fluid in a liquid storage tank is an important factor to consider when evaluating the serviceability of the structure, since sloshing waves can affect the functionality of the container and they can also lead to local damages of the tank.

In this Section, we determine analytically the frequencies of sloshing waves in the two-dimensional and three-dimensional containers described in the previous Sections. Subsequently, we investigate the capability of the system of resonators to limit the sloshing of the fluid contained in the tanks.

5.1 Analytical estimates of the frequencies of sloshing waves

The frequencies of sloshing waves in the fluid are calculated analytically in the framework of linear water wave theory, assuming that the walls of the container are rigid. The continuity equation and the linearised Navier-Stokes

equations are given by

$$\nabla \cdot \mathbf{v}_f = 0, \quad (16a)$$

$$\frac{\partial \mathbf{v}_f}{\partial t} + \frac{\nabla p}{\rho_f} = -g \mathbf{k}. \quad (16b)$$

We recall that ρ_f , \mathbf{v}_f , p , g and \mathbf{k} are the density of the fluid, the velocity field, the pressure, the acceleration of gravity and the unit vector in the direction normal to the free surface, respectively. The boundary conditions in a rigid container are expressed by

$$\mathbf{v}_f \cdot \mathbf{n} = 0 \quad \text{on the rigid walls,} \quad (17a)$$

$$p = p_0 \quad \text{on the free surface,} \quad (17b)$$

where p_0 is the atmospheric pressure and \mathbf{n} is the unit vector normal to the rigid walls.

Considering an irrotational flow, it is possible to define a velocity potential φ such that $\mathbf{v}_f = \nabla \varphi$. Assuming small perturbations of the free surface, the equations of the system and the boundary conditions become (see also Ibrahim (2005)):

$$\nabla^2 \varphi = 0 \quad \text{inside the fluid,} \quad (18a)$$

$$\nabla \varphi \cdot \mathbf{n} = 0 \quad \text{on the rigid walls,} \quad (18b)$$

$$\nabla \varphi \cdot \mathbf{n} = \frac{\omega^2 \varphi}{g} \quad \text{on the free surface,} \quad (18c)$$

where ω is the radian frequency. The solution of the linear water waves problem, defined by Eqs. (18), provides the radian frequencies of sloshing waves. We are interested, in particular, in the frequencies of sloshing waves relative to antisymmetric modes, which are the only modes that are excited when the fluid-solid system is subjected to ground shaking.

The radian frequencies of sloshing waves in the two-dimensional rectangular container examined in Section 3 are given by (Ibrahim (2005); Li and Wang (2012))

$$\omega_{(n)}^{2D} = \sqrt{g \beta_n \tanh(\beta_n h_W)} \quad \text{with} \quad \beta_n = \frac{n\pi}{2l_T} \quad (n = 1, 2, \dots), \quad (19)$$

where l_T and h_W are the half-width of the container and the height of the fluid, respectively. The first three frequencies of sloshing waves associated

with antisymmetric modes are $f_{(1)}^{2D} = 0.3951$ Hz, $f_{(3)}^{2D} = 0.6844$ Hz and $f_{(5)}^{2D} = 0.8835$ Hz, where $f_{(n)}^{2D} = \omega_{(n)}^{2D}/(2\pi)$. The same values have been obtained from a finite element model developed in *Comsol Multiphysics*[®].

For what concerns the three-dimensional cylindrical tank studied in Section 2, the radian frequencies have the following expressions (Ibrahim (2005)):

$$\omega_{(mn)}^{3D} = \sqrt{\frac{g\xi_{mn}}{r} \tanh\left(\frac{\xi_{mn}h_P}{r}\right)} \quad \text{with} \quad \xi_{mn} = \lambda_{mn}r \quad (m, n = 1, 2, \dots), \quad (20)$$

where r is the radius of the cylinder, h_P is the height of the fluid and λ_{mn} are the roots of the equation

$$\left. \frac{\partial J_m(\lambda_{mn}\rho)}{\partial \rho} \right|_{\rho=r} = 0, \quad (21)$$

being J_m the Bessel function of the first kind of order m . With the values assigned to the parameters in Section 2, the first three frequencies of sloshing waves related to antisymmetric modes are found to be $f_{(11)}^{3D} = 0.338$ Hz, $f_{(31)}^{3D} = 0.511$ Hz and $f_{(12)}^{3D} = 0.576$ Hz, where $f_{(mn)}^{3D} = \omega_{(mn)}^{3D}/(2\pi)$. Also in this case, the finite element model built in *Comsol Multiphysics*[®] provides a very accurate estimate of the analytical results.

If we consider an elastic container, namely if Eq. (17a) is substituted by Eq. (6a), the frequencies of sloshing waves decrease very slightly (as also found experimentally by Jiang et al. (2014)). The reason is that, both in the two-dimensional and in the three-dimensional cases, the deformations of the container are very small at those frequencies. Accordingly, we have not considered the frequencies of sloshing waves as eigenfrequencies of the fluid-solid system.

5.2 Sloshing waves in the two-dimensional container

We carry out numerical simulations in the transient regime for the two-dimensional container examined in Section 3. We impose a sinusoidal displacement at the bottom of the foundation, having a frequency equal to one of the frequencies of sloshing waves. Then, we determine the vertical displacement u_y of a point of the fluid close to the boundary with the solid, indicated by a black dot in the insets of Fig. 15.

The time-histories of u_y at 0.395 Hz and 0.684 Hz, which are the frequencies of the first and second antisymmetric modes of sloshing waves, are plotted by solid lines in Fig. 15a and 15b. The amplitudes of the applied displacement are 0.05 m and 0.04 m, respectively. For these simulations, the finite element software *Abaqus*[®] (version 6.14-4) has been used. The deformations of the fluid at different instants of time are shown in the insets of the diagrams, where the shapes of the first and second modes are clearly identified. For both frequencies, the level of the fluid increases unbounded with time due to resonance. In reality, the viscosity of the fluid would limit the increase in amplitude of sloshing waves.

The dotted lines in Figs. 15a and 15b represent the time-histories of u_y when the resonators are installed in the system. It is apparent that the resonators do not significantly modify the amplitudes of sloshing waves, therefore they result to be inefficacious to reduce the sloshing in the fluid. The reason is that at these frequencies the displacements of the container walls are very small, so that the container behaves as a rigid body and the resonators cannot divert the energy from the fluid.

5.3 Sloshing waves in the three-dimensional tank

We perform transient regime simulations for the three-dimensional container examined in Section 2. A sinusoidal displacement is imposed at the bottom of the foundation with a frequency corresponding to the first antisymmetric mode of sloshing waves (equal to 0.338 Hz) and with an amplitude equal to 0.02 m. Using the finite element software *Abaqus*[®], we compute the difference between the vertical displacements u_z of the two points of the fluid free surface close to the boundary with the solid, indicated by the black dots in the inset of Fig. 16. The time-history of the difference Δu_z is plotted by a solid line in Fig. 16.

The deformations of the fluid at different instants of time are shown in the insets of the diagram, where the shapes of the first mode are clearly identified. Moreover, we can note that the level of the fluid increases unbounded with time due to resonance.

The dotted line in Fig. 16 represents the time-history of Δu_z when the resonators are installed in the system. Similarly to the two-dimensional case, we can note that at this frequency the container behaves as a rigid body and the resonators do not significantly modify the amplitudes of sloshing waves. This result confirms that the resonators are not useful for the reduction of the

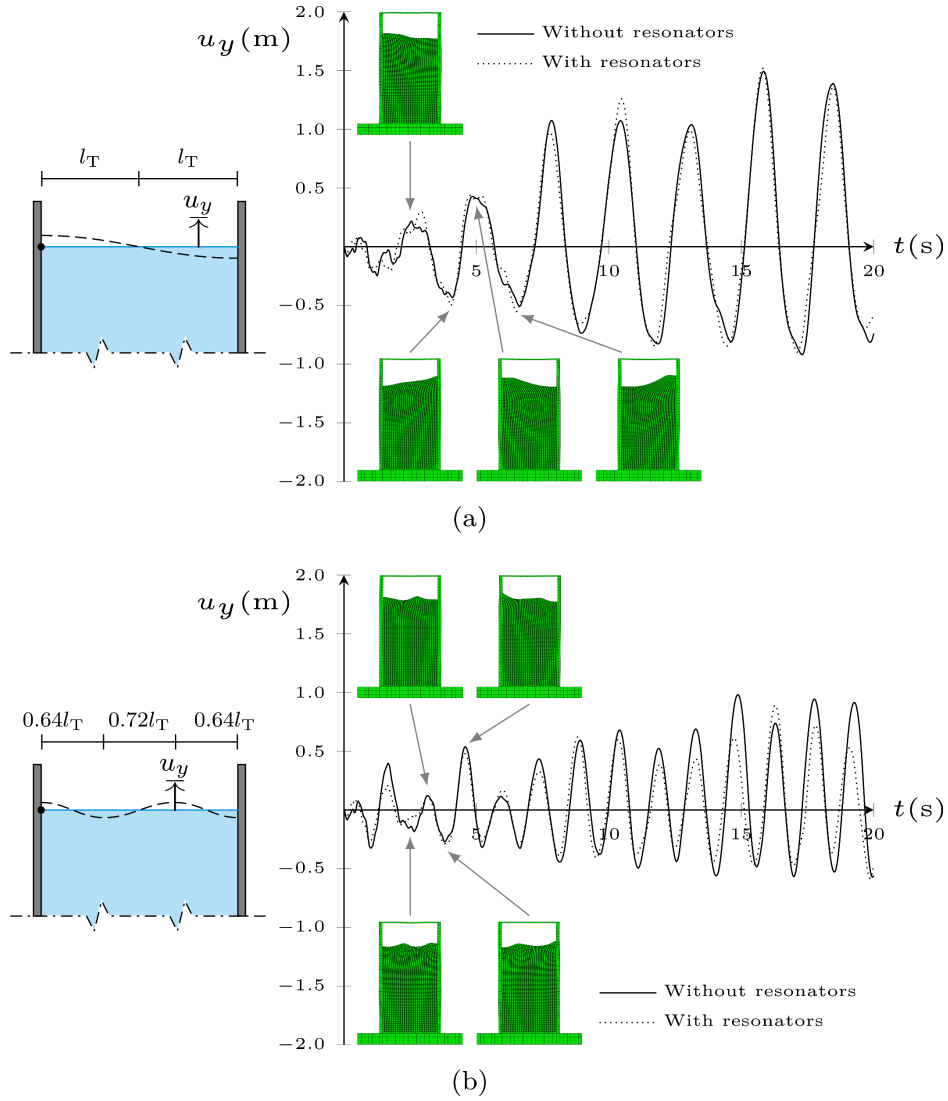


Figure 15: Time-histories of the vertical displacement u_y of the fluid point indicated by the black dot in the schematic representation on the left, computed at the frequencies 0.395 Hz (a) and 0.684 Hz (b). The solid and dotted lines refer to the cases without and with resonators, respectively.

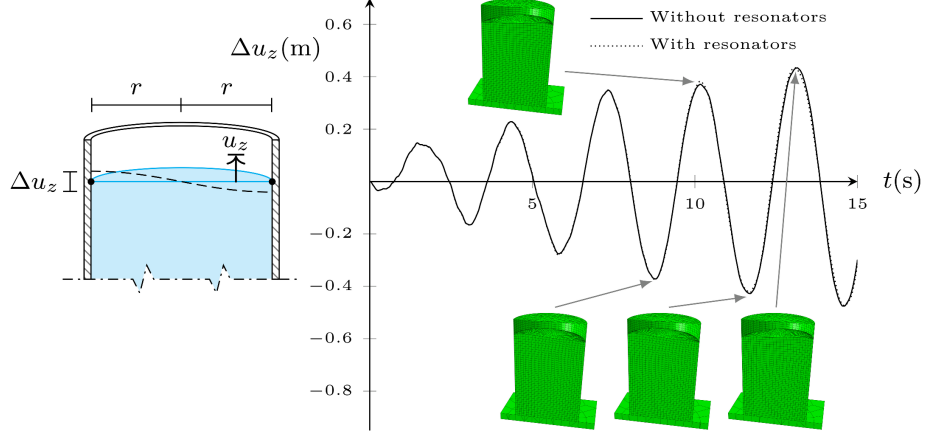


Figure 16: Time-histories of the difference Δu_z between the vertical displacements of the fluid points indicated by the black dots in the schematic representation on the left, computed at the frequency 0.338 Hz. The solid and dotted lines refer to the cases without and with resonators, respectively.

amplitudes of sloshing waves; to achieve this objective, the simplest solution is to introduce baffles (Belakroum et al. (2010); Wang et al. (2012)), which do not affect the properties of the resonators.

Finally, we observe that if the structure were more flexible, the frequencies of sloshing waves and the eigenfrequencies of the filled-fluid container would be closer. In this case, sloshing waves could increase the vibrations of the structure and viceversa. In such a system, the resonators would be very useful, as they would reduce the oscillations of the container and, as a consequence, the amplitudes of sloshing waves would not be increased by the structural vibrations.

6 Conclusions

The paper has presented an innovative design for isolation of vibrations of multi-scale structures consisting of fluid-filled containers. The idea of employing high-contrast multi-scale resonators has proved to be elegant and efficient to reduce vibrations of elastic containers filled with fluid within a predefined interval of frequencies. Another example of the effectiveness of the resonators for a large cluster of containers is illustrated in Fig. 17, where it is shown that in the system with resonators the vibration amplitudes are

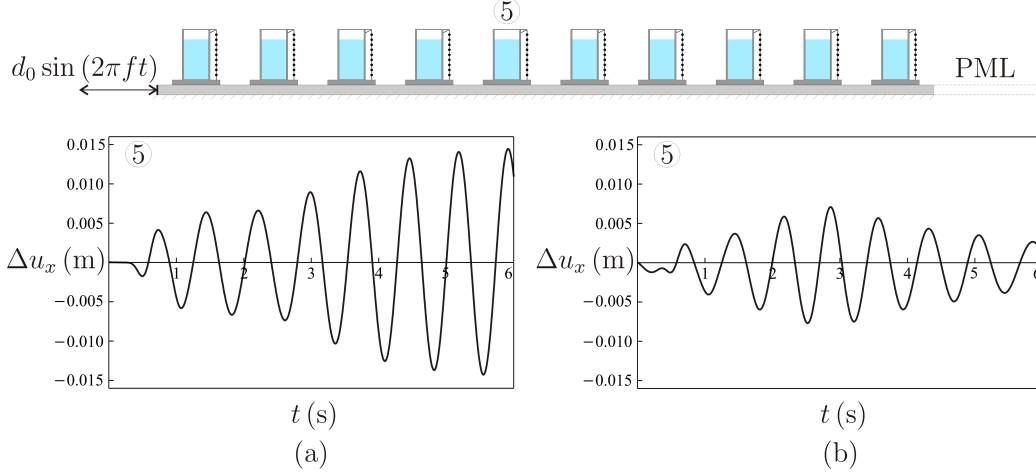


Figure 17: Relative displacement between the top and the bottom of the fifth container in a large system of fluid-filled containers, excited by a harmonic horizontal displacement $d_0 \sin(2\pi ft)$ with frequency $f = 1.35$ Hz, in the case without resonators (a) and in the presence of resonators (b). The capability of the resonators to reduce the vibrations of the system is evident.

decreased considerably and resonant effects in the main structure disappear.

The analytical estimates for the choice of parameters of the resonators have been based on the Floquet-Bloch approach, which provides a constructive guidance for the design of the multi-scale resonators. The numerical simulations have been carried out in the full fluid-solid interaction mode, with the fluid velocity and pressure satisfying the Navier-Stokes equations. Frequency response analyses have been performed in the framework of the linear water wave theory, and their results have been confirmed by transient simulations both in two and three dimensions.

In the practical implementation, viscous energy dissipating dampers are desirable and to be attached to the multi-scale resonators system. The current design clearly identifies the “energy sink”, and channels the energy of vibrations away from the main body of the fuel tank. The combined system, which includes viscous dampers, complements the design to the level of robust practical implementation.

The mass of the resonators and the stiffness of the connecting flexural links can be changed without affecting the dispersion properties of the Floquet-Bloch waves, as described in the analytical model presented in the main text of the paper. Hence, depending on the power of the external wave, the

resonators can be chosen to be heavier or lighter, in order to absorb the required amount of energy from the vibrating fuel container.

The model has high potential impact on industrial applications, concerning in particular the protection of fuel storage tanks in petrochemical plants subjected to seismic waves.

Acknowledgments

G.C. acknowledges the support from the Research Fund for Coal and Steel of the European Commission, INDUSE-2-SAFETY project, grant number RFSR-CT-2014-00025. L.A. would like to thank the University of Liverpool for financial support and provision of excellent research facilities. A.B.M. would like to thank the EPSRC (UK) for its support through Programme grant no. EP/L024926/1.

References

- Banerjee, S., Kundu, T., 2007. Ultrasonic field modeling in plates immersed in fluid. *Int. J. Solids Struct.* 44, 6013-6029.
- Belakroum, R., Kadja, M., Mai, T.H., Maalouf, C., 2010. An efficient passive technique for reducing sloshing in rectangular tanks partially filled with liquid. *Mech. Res. Commun.* 37, 341-346.
- Bursi, O.S., Abbiati, G., Caracoglia, L., La Salandra, V., Di Filippo, R., Reza, M.S., 2015. Dynamic response of coupled tanks and piping systems under seismic loading, in: 2015 ASME Pressure Vessels & Piping Conference, Boston.
- Carta, G., Brun, M., Movchan, A.B., 2014a. Dynamic response and localization in strongly damaged waveguides. *Proc. R. Soc. Lond. A* 470, 20140136.
- Carta, G., Brun, M., Movchan, A.B., Movchan, N.V., Jones, I.S., 2014b. Dispersion properties of vortex-type monatomic lattices. *Int. J. Solids Struct.* 51(11-12), 2213-2225.
- Carta, G., Brun, M., Movchan, A.B., Boiko, T., 2016. Transmission and localisation in ordered and randomly-perturbed structured flexural systems. *Int. J. Eng. Sci.* 98, 126-152.

- Cho, D.S., Kim, B.H., Kim, J.-H., Vladimir, N., Choi, T.M., 2015. Frequency response of rectangular plate structures in contact with fluid subjected to harmonic point excitation force. *Thin Wall. Struct.* 95, 276-286.
- Frandsen, J.B., 2004. Sloshing motions in excited tanks. *J. Comput. Phys.* 196(1), 53-87.
- Fuller, C.R., Fahy, F.J., 1982. Characteristics of wave propagation and energy distributions in cylindrical elastic shells filled with fluid. *J. Sound Vib.* 81(4), 501-518.
- Graham, E.W., Rodriguez, A.M., 1952. The characteristics of fuel motion which affect airplane dynamics. *J. Appl. Mech.* 19(3), 381-388.
- Housner, G.W., 1957. Dynamic pressures on accelerated fluid containers. *Bull. Seism. Soc. Am.* 47(1), 15-35.
- Housner, G.W., 1963. The dynamic behavior of water tanks. *Bull. Seism. Soc. Am.* 53(2), 381-387.
- Ibrahim, R.A., 2005. *Liquid Sloshing Dynamics: Theory and Applications*, Cambridge University Press, Cambridge.
- Jiang, M.-R., Ren, B., Wang, G.-Y., Wang, Y.-X., 2014. Laboratory investigation of the hydroelastic effect on liquid sloshing in rectangular tanks. *J. Hydrodyn.* 26(5), 751-761.
- Krausmann, E., Cruz, A.M., Affeltranger, B., 2010. The impact of the 12 May 2008 Wenchuan earthquake on industrial facilities. *J. Loss Prev. Process Ind.* 23, 242-248.
- Kuznetsov, N., Maz'ya, V., Vainberg, B., 2002. *Linear Water Waves: A Mathematical Approach*, Cambridge University Press, Cambridge.
- Li, Y., Wang, J., 2012. A supplementary, exact solution of an equivalent mechanical model for a sloshing fluid in a rectangular tank. *J. Fluids Struct.* 31, 147-151.
- Li, Y., Di, Q., Gong, Y., 2012. Equivalent mechanical models of sloshing fluid in arbitrary-section aqueducts. *Earthquake Eng. Struct. Dyn.* 41, 1069-1087.

- Liao, C.-Y., Ma, C.-C., 2016. Vibration characteristics of rectangular plate in compressible inviscid fluid. *J. Sound Vib.* 362, 228-251.
- Mead, D.M., 1996. Wave propagation in continuous periodic structures: Research contributions from Southampton, 1964-1995. *J. Sound Vib.* 190(3), 495-524.
- Mencik, J.-M., Ichchou, M.N., 2007. Wave finite elements in guided elastodynamics with internal fluid. *Int. J. Solids Struct.* 44, 2148-2167.
- Païdoussis, M.P., 1998. *Fluid-Structure Interactions: Slender Structures and Axial Flow*, Vol. 1, Academic Press, San Diego.
- Païdoussis, M.P., 2004. *Fluid-Structure Interactions: Slender Structures and Axial Flow*, Vol. 2, Elsevier Academic Press, London.
- Pal, P., Bhattacharyya, S.K., 2010. Sloshing in partially filled liquid containers - Numerical and experimental study for 2-D problems. *J. Sound Vib.* 329, 4466-4485.
- Sorokin, S.V., Nielsen, J.B., Olhoff, N., 2004. Green's matrix and the boundary integral equation method for the analysis of vibration and energy flow in cylindrical shells with and without internal fluid loading. *J. Sound Vib.* 271, 815-847.
- Ursell, F., 1958. *Forced small-amplitude water waves: A comparison of theory and experiment*, Massachusetts Institute of Technology Hydrodynamics Laboratory, Boston.
- Ursell, F., 1994. *Ship Hydrodynamics, Water Waves and Asymptotics*, World Scientific, Singapore.
- Veletsos, A.S., 1984. Seismic response and design of liquid storage tanks, in: *Guidelines for the Seismic Design of Oil and Gas Pipeline Systems*. ASCE, New York, pp. 255-370.
- Wang, J.D., Lo, S.H., Zhou, D., 2012. Liquid sloshing in rigid cylindrical container with multiple rigid annular baffles: Free vibration. *J. Fluids Struct.* 34, 138-156.

Washizu, K., Nakayama, T., Ikegawa, M., Tanaka, Y., Adachi, T., 1984. Some finite element techniques for the analysis of non-linear sloshing problems, in: Gallagher, R.H., Oden, J.T., Zienkiewicz, O.C., Kawahara, M. (Eds.), Finite Elements in Fluids. John Wiley, New York, pp. 357-376.